Sheep liver cytosolic aldehyde dehydrogenase: the structure reveals the basis for the retinal specificity of class 1 aldehyde dehydrogenases

Stanley A Moore[1], Heather M Baker[1†], Treena J Blythe[1], Kathryn E Kitson[2], Trevor M Kitson[3] and Edward N Baker[1†*]

Background: Enzymes of the aldehyde dehydrogenase family are required for the clearance of potentially toxic aldehydes, and are essential for the production of key metabolic regulators. The cytosolic, or class 1, aldehyde dehydrogenase (ALDH1) of higher vertebrates has an enhanced specificity for all-*trans* retinal, oxidising it to the powerful differentiation factor all-*trans* retinoic acid. Thus, ALDH1 is very likely to have a key role in vertebrate development.

Results: The three-dimensional structure of sheep ALDH1 has been determined by X-ray crystallography to 2.35 Å resolution. The overall tertiary and quaternary structures are very similar to those of bovine mitochondrial ALDH (ALDH2), but there are important differences in the entrance tunnel for the substrate. In the ALDH1 structure, the sidechain of the general base Glu268 is disordered and the NAD^+ cofactor binds in two distinct modes.

Conclusions: The submicromolar K_m of ALDH1 for all-*trans* retinal, and its 600-fold enhanced affinity for retinal compared to acetaldehyde, are explained by the size and shape of the substrate entrance tunnel in ALDH1. All-*trans* retinal fits into the active-site pocket of ALDH1, but not into the pocket of ALDH2. Two helices and one surface loop that line the tunnel are likely to have a key role in defining substrate specificity in the wider ALDH family. The relative sizes of the tunnels also suggest why the bulky alcohol aversive drug disulfiram reacts more rapidly with ALDH1 than ALDH2. The disorder of Glu268 and the observation that NAD^+ binds in two distinct modes indicate that flexibility is a key facet of the enzyme reaction mechanism.

Addresses: [1]Institute of Molecular Biosciences, Massey University, Private Bag 11-222, Palmerston North, New Zealand, [2]Institute of Food, Nutrition and Human Health, Massey University, Private Bag 11-222, Palmerston North, New Zealand and [3]Institute of Fundamental Sciences, Massey University, Private Bag 11-222, Palmerston North, New Zealand.

[†]Present address: School of Biological Sciences, University of Auckland, Auckland, New Zealand.

*Corresponding author.
E-mail: Ted.Baker@Auckland.ac.nz

Keywords: aldehyde dehydrogenase, crystal structure, cytosolic, nicotinamide adenine dinucleotide, retinal, retinoic acid

Received: 18 August 1998
Revisions requested: 10 September 1998
Revisions received: 2 October 1998
Accepted: 5 October 1998

Structure 15 December 1998, 6:1541–1551
http://biomednet.com/elecref/0969212600601541

Introduction

The retinoic acid signalling pathway in vertebrates utilises the RXR/RAR family of ligand-dependent transcription factors that bind 9-*cis* (RXR,RAR) or all-*trans* (RAR) retinoic acid via a ligand-binding domain, and direct the transcription of target genes via a DNA-binding domain [1,2]. Retinoic acid is derived from vitamin A (retinol) and its pleiotropic effects include spinal chord and retina development during embryogenesis, neuronal cell differentiation and maintenance of epithelial cell type in adult tissues [3]. Although the retinoic acid signalling pathway is reasonably well understood, it is less clear how spatiotemporal gradients of retinoic acid are maintained during developmental processes, and which are the major enzymes responsible for retinoic acid synthesis in various tissues [4].

The cloning and characterisation of several aldehyde dehydrogenases (ALDHs) showing a high specificity for retinaldehyde has recently been reported. Each of these enzymes has been shown to belong to the broad family of cytosolic or class 1 ALDH (ALDH1) enzymes [4,5]. Studies on mouse embryos show that retinaldehyde-specific ALDH activity co-localises with high concentrations of retinoic acid in the developing spinal chord [6], and retinaldehyde dehydrogenase is a positional marker in the mouse embryonic retina [7]. Retinal-specific ALDHs can be divided into three groups on the basis of their amino acid sequence and pI values [5]. The archetypal class 1 ALDH is found predominantly in the liver of higher vertebrates including horse, beef, sheep and man, and has a pI of 5.2. Two retinal-specific variants of ALDH1 (RalDH-1 and -2) have been characterised in the mouse and rat, but not in other mammals. One of these, RalDH-1, is about 90% identical to the other class 1 enzymes, has a pI of ~8.3 [7–10], and effectively converts both 9-*cis* and all-*trans* retinal to the corresponding retinoic acid [11,12]. The other enzyme, RalDH-2, is only about 70% identical to the classical ALDH1 enzymes, has a pI of 5.1, and is specific for oxidising retinaldehyde [13,14].

ALDHs are found in most mammalian tissues. In humans alone, eight distinct ALDH alleles have been characterised [15]. The liver has high ALDH activity, and in this tissue there are two principal isozymes, ALDH1 and ALDH2.

ALDH1 is cytosolic and ALDH2 is produced with a leader peptide sequence and targeted to the mitochondrial matrix. Human ALDH1 has been shown to have a submicromolar K_m for both all-*trans* retinal [16,17] and 9-*cis* retinal [5]. Kinetic studies of sheep ALDH1 indicate that it has a high specific activity for both all-*trans* and 9-*cis* retinal, with a K_m value of 0.14 μM for both substrates [5]. Acetaldehyde is a much poorer substrate for human ALDH1, with a K_m of 180 μM [18]. In contrast, kinetic data suggest that acetaldehyde is the preferred substrate of human ALDH2, having a K_m value of 0.2 μM [18]. The presence of an alcohol-sensitivity phenotype mapping to the human ALDH2 locus [19–22] strongly indicates that the major biological function of ALDH2 is to metabolise ethanol-derived acetaldehyde. Human ALDH2 also has essentially no activity for all-*trans* retinaldehyde [16], underscoring the complementary substrate specificity of these two enzymes.

Both ALDH1 and ALDH2 are homotetramers comprising subunits of 500 or 501 amino acids, and they require nicotinamide adenine dinucleotide (NAD^+) as a cofactor [15]. The aligned ALDH1 and ALDH2 amino acid sequences are approximately 69% identical, suggesting a high similarity of their three-dimensional structures. The inducible ALDH3 family of enzymes is much more distantly related to ALDH1 and ALDH2, being only 30% identical at the amino acid level, and lack an N-terminal segment present in ALDH1 and ALDH2. In addition, whereas ALDH1 and ALDH2 are homotetramers, ALDH3 is dimeric [23].

The enzymology and kinetics of sheep liver ALDH1 have been investigated in detail [5,24–27]. For both ALDH1 and ALDH2, the dehydrogenase reaction follows an ordered sequential pathway [24]. NAD^+ binds first, followed by binding of the aldehyde and formation of a thiohemiacetal intermediate with the active-site nucleophile, which has been identified as Cys302 [28–31]. The thiohemiacetal then collapses to the thioester, giving up a hydride ion to C4 of the nicotinamide ring of NAD^+ in the process. Hydride transfer has been shown to be stereospecific for the class 3 enzymes, adding only to the Pro-R or A-side of the nicotinamide ring [32]. The thioester is presumably hydrolysed by a water molecule, which becomes activated by the general base Glu268 [28,33,34]. Release of the carboxylic acid, followed by NADH release, completes the reaction.

We have undertaken structural studies of sheep liver ALDH1 in order to better understand the differences in substrate specificity between ALDH1 and ALDH2, and to obtain a clearer overall view of the mechanism and function of this important family of enzymes. In particular, we hoped to learn more about the role of ALDH1 in retinoic acid synthesis. Our results will complement structural studies on other proteins involved in retinoid metabolism, including those on the ligand-binding domain of the retinoic acid receptor [35,36], and cellular proteins that bind retinol [37,38] and retinoic acid [39,40].

Results

Structure solution and refinement

The three-dimensional structure of sheep liver ALDH1 was first solved by molecular replacement using the bovine ALDH2 atomic coordinates as a search model. After refinement against diffraction data in a triclinic unit cell (Table 1), the completed sheep ALDH1 model includes four polypeptides comprising an intact tetramer (each polypeptide contains 494 amino acids; the first seven amino acids are not included in our model due to apparent disorder), four NAD^+ cofactors and a total of 140 water molecules (see Table 2). The R factor is 23.6% for all data to 2.35 Å resolution; the R free is 25.8%. The overall stereochemistry for the ALDH1 atomic model is excellent with root mean square deviations (rmsds) from standard geometry being 0.009 Å (for bonds) and 1.61° (for angles) with no Ramachandran outliers. There are some local noncrystallographic symmetry (NCS) deviations, mostly due to small rigid-body movements of mainchain atoms or alternate sidechain conformers in the monomers. In this paper we use the consensus amino acid sequence numbering for ALDH1 and ALDH2 (e.g. Cys302, Glu268, etc.); this results in the amino acid sequence starting at –1 for sheep ALDH1. In addition, we make use of the secondary structure assignments for bovine ALDH2 [34], for consistency and ease of comparison of the two structures.

Overall structure of sheep ALDH1

A superposition of the refined sheep ALDH1 model on the bovine ALDH2 atomic coordinates yields an rmsd in mainchain atoms (N, Cα, C, O) of 0.74 Å for the entire polypeptide chain (Figure 1a). This result is not surprising, given that the sheep ALDH1 amino acid sequence [41] is about 69% identical to the bovine ALDH2 sequence. Omitting 16 outlying residues from the superposition increases the structural agreement markedly, the rms pairwise difference drops to 0.58 Å.

ALDH1 is made up of three domains: an N-terminal NAD^+-binding domain (residues 8–135 and 159–270) that is novel to the ALDH family and contains a five-stranded parallel β sheet [23,34]; a catalytic domain (residues 271–470) that contains a six-stranded parallel β sheet; and an oligomerisation domain made up of a three-stranded antiparallel β sheet (residues 140–158 and 486–495). Both the NAD^+-binding and catalytic domains are based on topologically related βαβ type polypeptide folds (Figure 1b).

The N-terminal NAD^+-binding domains of ALDH enzymes exhibit a unique mode of cofactor binding that appears to be distantly related to the canonical NAD-binding domain found in most NAD(P) utilising dehydrogenases, and has been discussed in detail [23,34]. The sheep ALDH1

Table 1

Data collection statistics.

	Native 1	Native 2
X-ray source	PF, BL6A	Rigaku RU-200
Detector used	Weissenberg	RAXIS-IIC
Temperature (K)	290	113
Diffraction limit (Å)	3.10	2.35
Number of reflections	20,519	83,641
Completeness (%)*	92.6 (82.1)	95.5 (93.7)
Overall redundancy*	3.0 (2.5)	2.7 (2.6)
I/σ*	7.0 (2.6)	11.3 (2.7)
R_{merge}*†	0.131 (0.319)	0.096 (0.350)
Space group	$P2_12_12$	P1
Asymmetric unit	Dimer	Tetramer
a axis (Å)	94.63	80.69
b axis (Å)	152.2	87.62
c axis (Å)	81.18	90.84
α (°)	90.00	110.5
β (°)	90.00	105.6
γ (°)	90.00	103.6

*Values in parentheses are for the highest resolution shell. †$R_{merge} = \Sigma|I-<I>|/\Sigma I$, where <I> is the mean of individual observations of intensities I. All unit-cell dimensions were determined by post-refinement within SCALEPACK, except for the Photon Factory (PF) data where the values were averaged from individual films.

Table 2

Model statistics.

Model	
No. of protein atoms	15,144
No. of water molecules	140
No. of cofactor atoms	176
Average B factors	
Mainchain atoms (Å^2)	28.1
Sidechain atoms (Å^2)	29.7
Cofactor atoms (Å^2)	34.3
Overall (Å^2)	29.4
Stereochemistry	
Root mean square deviations	
bond lengths (Å)	0.009
bond angles (°)	1.61
planar groups (Å)	0.018
bonded mainchain B factors (Å^2)	1.06
bonded sidechain B factors (Å^2)	1.82
angle mainchain B factors (Å^2)	1.66
angle sidechain B factors (Å^2)	2.58
Noncrystallographic symmetry	
Rms deviations	
mainchain atoms (Å)	0.009
sidechain atoms (Å)	0.090
NAD^+ atoms (Å)	0.030
Refinement	
R factor*	0.236
R free†	0.258

*The R factor was calculated using 74,932 reflections within the resolution range 100–2.35 Å. †The R free was calculated using 8274 reflections.

structure expands the generality of the unique ALDH NAD^+-binding motif, as the general mode of NAD^+ binding observed first in ALDH3 [23] and then ALDH2 [34] is conserved for the cofactor in our structure (Figure 1b).

The main differences in the ALDH1 and ALDH2 polypeptide conformations are localised to a particular region of the structure that is in the vicinity of the substrate entrance tunnel (Figures 1a and 2). In particular, residues 13–18 (rmsd 2.68 Å), residues 329–341 (rmsd 2.20 Å) and residues 371–382 (rmsd 1.18 Å) in sheep ALDH1 are displaced relative to the bovine ALDH2 structure. These regions do not themselves have secondary structure, but they do exert rigid-body displacements on α helices and β sheets that are adjacent in the primary sequence. Helix αJ (residues 347–364) is noteworthy because it makes up one side of the NAD^+-binding pocket, and is slightly displaced relative to bovine ALDH2 (rmsd 0.84 Å). The bottom of the substrate entrance tunnel makes up part of the tetramer interface (see Figure 2) and includes helix αM (residues 435–446, rmsd 0.91 Å) and the 468–469 peptide, both of which show displacements relative to ALDH2. Other structural perturbations are observed at the oligomerisation interface, including residues 139–140 and helix αN (residues 479–484, rmsd 1.14 Å).

The entrance tunnel for the retinal substrate

Certainly the most striking feature of the sheep ALDH1 three-dimensional structure is the large-scale change in the entrance tunnel for the substrate relative to ALDH2. The entrance to this tunnel is made up of two α helices and a surface loop (Figure 2). Helix αC (residues 114–135) makes up the left-hand side of the opening and forms part of a three-helix bundle near the beginning of the N-terminal domain. The back of the tunnel is made up by helix αD (residues 170–185), which incidentally packs against helix αC. Helix αD is also the first α helix of the canonical Rossmann fold of the N-terminal domain. Helix αH (residues 282–296) makes up the bottom of the substrate entrance tunnel, as viewed in Figure 2, and originates from the catalytic domain, immediately preceding the active-site nucleophile (Cys302). The right-hand side of the tunnel is made up of a surface loop (residues 455–461) that precedes helix αN near the oligomerisation domain (Figures 1 and 2), this loop rests against helix αH. The base of the tunnel comprises two β strands containing Thr244 and Glu268, respectively.

There are multiple amino acid substitutions between the ALDH1 and ALDH2 enzyme families that map to these portions of the structure, facing into the substrate access tunnel (Figure 2). These substitutions are generally obeyed

Figure 1

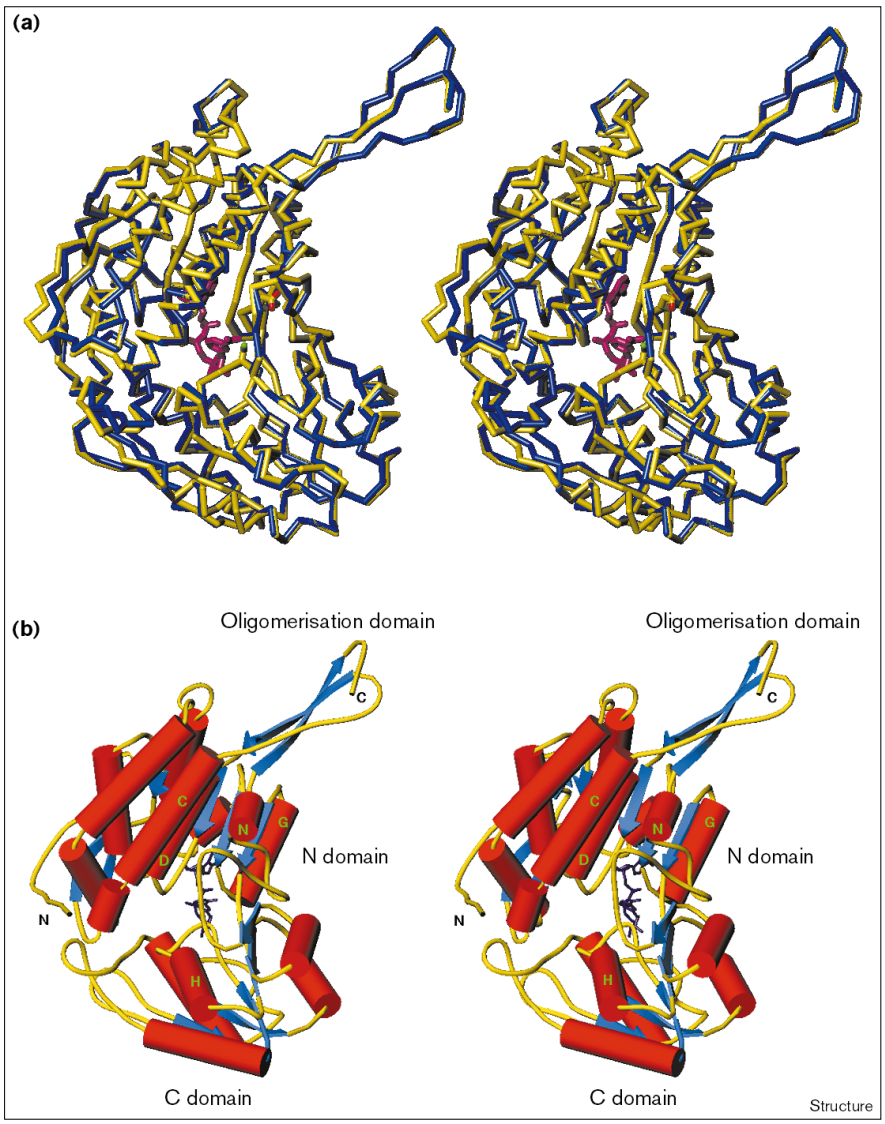

The overall fold of the ALDH1 monomer. (a) Stereoview superposition of a monomer of sheep ALDH1 (yellow) and bovine ALDH2 (blue). The pairwise root mean square difference is 0.74 Å using all mainchain atoms. (b) Schematic diagram of the sheep ALDH1 monomer looking into the substrate entrance tunnel. The NAD^+ (major conformation) is also shown as a purple stick model. Helices are shown as red cylinders and strands are shown as blue arrows. Secondary structure elements mentioned in the text are labelled. (The figure was created using the program TURBO-FRODO [61].)

in all ALDH1 (retinal metabolising) and ALDH2 (acetaldehyde metabolising) amino acid sequences. For helix αC, these substitutions, going from bovine ALDH2 to sheep ALDH1 respectively, are Pro113→Leu, Ile116→Asn, Val120→Met, Asp123→Gly, Met124→Gly, Cys128→Thr and Tyr132→Cys. Similarly, for helix αH, the observed substitutions are Trp285→Asn, Gln289→Phe, Phe292→Gln, Phe296→Tyr and Asn297→His. The substitutions in the surface loop preceding the oligomerisation interface are Asp457→Ser, Phe459→Val, Gly460→Ser and Leu482→Phe. In nine of these substitutions, the ALDH2 sidechains are bulkier than their ALDH1 counterparts, and they almost exclusively adopt conformations that result in a more constricted entrance tunnel than in ALDH1. Several amino acid sidechains that are identical in the ALDH1 and ALDH2 sequences again adopt conformations in ALDH2 that make the entrance tunnel smaller than in ALDH1 (Figure 2). Examples of such residues include Lys112, Met174, Trp177, Cys301 and Leu477; all of these residues have well-defined electron density and lower than average B factors in the four ALDH1 subunits. These two factors combine with the result that the ALDH1 entrance tunnel is much larger than that of bovine ALDH2, thereby allowing access to larger, more bulky substrates, such as all-*trans* retinal (Figure 2). In addition to amino acid substitutions, small but concerted rigid-body movements of secondary structure elements contribute to the opening up of the substrate tunnel in ALDH1 relative to ALDH2. Indeed, the solvent-accessible volume of the tunnel is 150 $Å^3$ in sheep ALDH1, but only 20 $Å^3$ in bovine ALDH2 (when using a 1.4 Å radius probe). These observations are in accord with all-*trans* retinal being a very good substrate for ALDH1, but

Figure 2

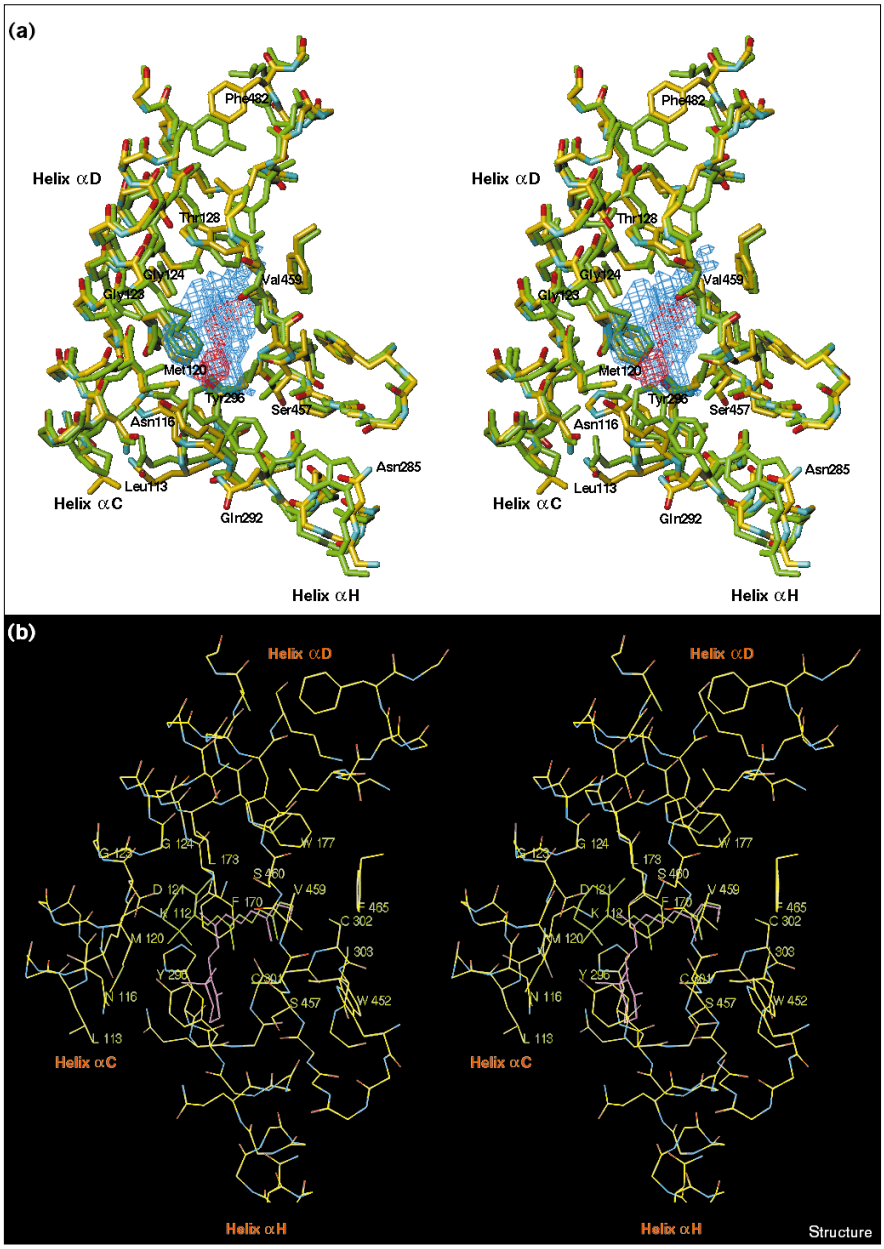

The substrate entrance tunnel of ALDH1. (a) Stereoview superposition of the active-site tunnel in ALDH1 (standard atom colours) and ALDH2 (green) showing the major differences in sidechain conformations between the two isozymes. Residues that are different in ALDH1 are labelled. The solvent-accessible volumes for ALDH1 and ALDH2 are shown in blue and red, respectively. (b) Stereoview showing the results of docking all-*trans* retinal (green) and 9-*cis* retinal (purple) in the ALDH1 active-site tunnel. The protein atoms are shown in standard colours; both protein and substrate are represented as stick models. (The figure was created using the program TURBO-FRODO [61].)

a very poor substrate for ALDH2 [16]. Modelling of either 9-*cis* or all-*trans* retinal into the ALDH1 active-site tunnel illustrates that the ALDH1 tunnel can easily accommodate either retinoid (Figure 2), but the tunnel in ALDH2 is too small to accommodate these bulky substrates and steric clashes result. In the substrate modelling experiment, the solvent-accessible surface area of the ALDH1 tunnel decreases by 333 Å^2 and that of all-*trans* retinal decreases by 520 Å^2. These values are comparable to the published buried surface areas of 279 Å^2 (for protein) and 558 Å^2 (for all-*trans* retinol) in the complex formed between cellular retinol-binding protein (CRBP) and retinol [37]. In both of our modelled complexes, the β-ionone ring of the retinal sticks out from the tunnel entrance and is partially exposed to solvent. This is in contrast to what is observed in complexes of CRBP and retinoic acid binding protein (CRABP) with their respective ligands. In these complexes, the β-ionone ring is buried to a greater extent and the solvent-accessible cavity for the ligand is much larger — 174 Å^3 and 280 Å^3 for CRBP and CRABP, respectively [37,40].

Discrete disorder of the NAD$^+$ cofactor

The adenine ring of the NAD$^+$ cofactor sits in a hydrophobic pocket between helices αF and αG (Figures 1b

and 3a) and its conformation is virtually identical to that of the adenine half of the NAD^+ observed in the ALDH3 [23] and ALDH2 [34] structures. As in ALDH2, the sidechains of amino acids Gly225, Pro226, Ala230, Val249, Leu252 and Ile253 cradle the adenine ring while the sidechain of Ile165 makes up the base of the cradle. Hydrogen-bonding interactions with the adenine ribose are made by the sidechains of Lys192, Glu195 and the mainchain carbonyl oxygen of Ile166 in both the ALDH1 and ALDH2 structures (Figure 3a).

In contrast, the nicotinamide half of the NAD^+ cofactor is strikingly different from that observed in ALDH3 and ALDH2, and there is evidence of discrete disorder in the nicotinamide half of NAD^+ (Figure 3). After modelling and refinement of the major NAD^+ conformer (Figure 3), a tetrahedral-shaped difference electron-density peak was observed in $|F|_{obs}-|F|_{calc}$ maps. This peak was large enough at the 5σ level to accommodate a phosphate anion, but made bad steric clashes with the position of the modelled nicotinamide ring. The large difference peak was persistent, and once the ALDH2 NAD^+ coordinates were superimposed onto the sheep ALDH1 model, the ALDH2 nicotinamide phosphate was found to be coincident with our large difference electron-density peak. Hence, we concluded that the large difference peak must be due to a second, more weakly occupied conformation of the nicotinamide phosphate. Indeed, when the major NAD^+ conformer is omitted from the model, there is weaker discontinuous $|F|_{obs}-|F|_{calc}$ difference electron density at the 3σ level corresponding to the ribose and some of the nicotinamide of the 'second' conformation that almost exactly overlaps with the atomic coordinates for the nicotinamide half of the ALDH2 NAD^+ (Figure 3b). We conclude that the sheep ALDH1 structure contains two major conformations of the nicotinamide half of the NAD^+. The less occupied conformation corresponds to the NAD^+ conformation observed in the bovine ALDH2 structure [34].

Differences between the two NAD^+ orientations are first seen at the phosphate attached to the adenine ribose (Figure 3b). In ALDH1, the adenine phosphate O1 atom makes two hydrogen bonds: one with Ser246 Oγ and the other with Ser246 N. The slight reorientation of the adenine phosphate seen in our structure pivots the major conformer of the nicotinamide phosphate to be displaced relative to that observed in bovine ALDH2. In ALDH1 we see a hydrogen bond between Trp168 Nε1 and the O5 atom of the nicotinamide phosphate, whereas in ALDH2 it is O4 of the phosphate that is hydrogen bonded to Trp168 Nε1.

The reorientation of the major NAD^+ conformer observed in our structure results in a movement of over 5 Å for the nicotinamide ribose relative to bovine ALDH2. Indeed, the nicotinamide ring of ALDH1 occupies nearly the same position as the nicotinamide ribose of ALDH2 (Figure 3b). Interactions between the nicotinamide ribose and the protein involve Gln349, Glu399 and Phe401, as in ALDH2, but the hydrogen bonds and van der Waals contacts that they form are strikingly different (see Figure 3a). Hence, the same amino acid residues participate in nicotinamide binding in both ALDH1 and ALDH2, but they do so in a distinctly different manner. In addition, the sidechain of Lys352 makes hydrogen-bond interactions with the nicotinamide ribose oxygen atoms in the ALDH1 structure, but this is not observed in ALDH2. The end result is that in the ALDH1 crystal structure, the C4 atom of the nicotinamide is too far from Cys302 Sγ (7.1 Å in ALDH1 versus 3.7 Å in ALDH2) for direct hydride transfer from a thiohemiacetal intermediate to occur during the dehydrogenase reaction. Hence, we are likely to be looking at a catalytically nonproductive mode of cofactor binding in the major NAD^+ conformer.

The environment of Cys302 and other active-site residues

Although the ALDH1 and ALDH2 structures superimpose well, the orientations of several sidechains at the active site differ in the two ALDH isozymes (Figure 2). Of particular note is Cys301, which directly precedes the active-site nucleophile Cys302. In sheep liver ALDH1, χ_1 for Cys301 is –60°, whereas in bovine ALDH2 it is 180°, putting the Sγ atom much closer to the Sγ atom of Cys302. Other sidechains that exhibit different conformations are Lys112, Met174 and Trp177, all of which line the active-site pocket (Figure 2). On the opposite side of the active site from Cys302 is an ion pair formed between Lys178 and Glu476; these two amino acids are conserved in the sequences of all tetrameric ALDHs. The sidechains of both of these residues are in slightly different orientations in sheep ALDH1 relative to bovine ALDH2.

Not only are there differences in the sidechain conformations of several conserved amino acids at the active site, but there are also a number of amino acid substitutions in ALDH1 compared to ALDH2. Included in these are Phe289, Gln292, Tyr296, His297, Ile303, Ser428, Ser457, Val459 and Ser460, but most of these have been mentioned with respect to differences in the substrate entrance tunnels of the two enzymes (Figure 2).

Possible flexibility of the general base Glu268

Mutagenesis experiments with human liver ALDH2 have shown that Glu268 acts as a general base in both thiohemiacetal formation and thioester hydrolysis [33]. Although the Glu268 sidechain in our ALDH1 structure is modelled as the same rotamer as observed in bovine ALDH2, it exhibits unexpectedly weak electron density (Figure 4) and high B factors for a residue buried from solvent (average B factor 41 $Å^2$ compared to neighbouring amino acids with average B factors of ~25 $Å^2$). There is no $2F_o-F_c$ or difference electron density for the Cα–Cβ bond if the Glu268 sidechain is

Figure 3

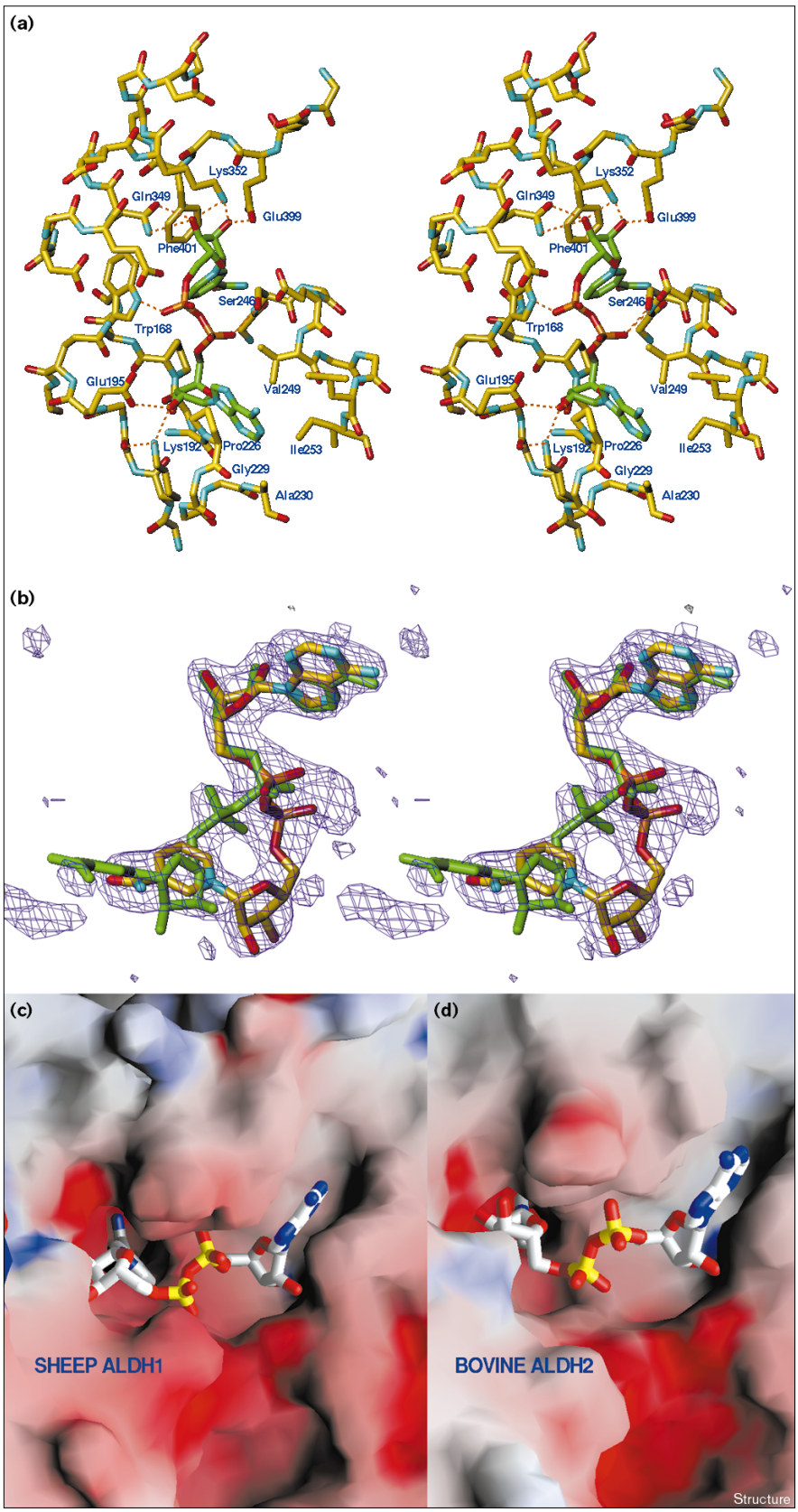

NAD^+ binding in ALDH1. (a) Stereoview illustrating the major NAD^+-binding mode in ALDH1. Key residues of the protein are labelled and hydrogen bonds are shown as dashed lines. Carbon atoms of the protein are shown in yellow and those of NAD^+ are in green; other atoms are in standard colours. (b) Stereoview omit map of the NAD^+-binding region in ALDH1. The refined coordinates of the ALDH1 NAD^+ molecule (in standard atom colours) are shown superimposed with the ALDH2 NAD^+ molecule (in green). The map is contoured at 3σ and has not been cushioned or cosmetically altered. Surface representations of (c) the ALDH1 and (d) the ALDH2 monomers in the vicinity of the NAD^+-binding site, coloured by electrostatic potential. Bound NAD^+ is shown in stick representation. Note the large region of negative electrostatic potential near the NAD^+ pyrophosphate. (Figures (a) and (b) were generated using the program TURBO-FRODO [61]; figures (c) and (d) were generated using the program GRASP [62].)

Figure 4

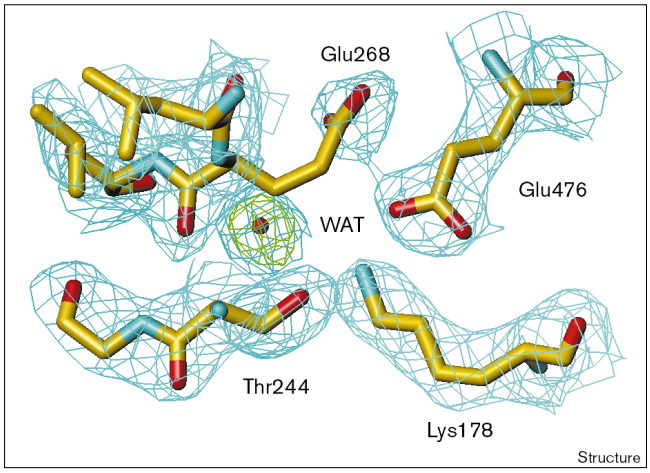

A view of ALDH1 showing the $2F_o–F_c$ electron density in blue contoured at 0.9σ in the vicinity of Glu268. $F_o–F_c$ density for a possible deacylating water molecule is shown in green at 3.0σ. (The figure was created using the program TURBO-FRODO [61].)

removed during least squares refinement. Glu268 is likely to be hydrogen bonded to the nicotinamide ring amide nitrogen of our low occupancy nicotinamide conformer, as observed in ALDH2, or to a higher occupancy water molecule ~4 Å from the Glu268 carboxylate in ALDH1 (shown as a green difference electron-density peak in Figure 4). However, the height of this water peak varies in each of our four independent active sites, suggesting variable occupancy. We have therefore not included this potential water molecule in our refined model. If this was the deacylating water molecule for ALDH1, it is difficult to imagine how it would be held in place as it makes no good hydrogen bonds with the protein. However, it is positioned approximately the correct distance from Cys302 Sγ to hydrolyse the envisaged thioester intermediate.

Discussion

The substrate entrance tunnel

The obvious difference in the size and shape of the substrate entrance tunnel of ALDH1 relative to ALDH2 reinforces what is known about the substrate specificities of these enzymes. The ALDH1 tunnel is more open than its counterpart in ALDH2, and hence ALDH1 must clearly accommodate larger, bulkier substrates than ALDH2. ALDH1 prefers retinal as a substrate, whereas ALDH2 prefers acetaldehyde. In fact, the converse is also true as retinal is a poor substrate of ALDH2, and acetaldehyde is a relatively poor substrate of ALDH1.

The size of the substrate entrance tunnel may also explain the differential reactivities of ALDH1 and ALDH2 towards the ALDH inhibitor disulfiram. Disulfiram is a bulky, hydrophobic compound that reacts quickly with ALDH1 and more slowly with ALDH2 [42–44]. We anticipated that the ALDH1 active site would be more hydrophobic than that of ALDH2, but in fact there are more polar residues lining the ALDH1 substrate entrance tunnel. As in the case of retinal, we conclude that it is more likely to be the size and shape of the substrate entrance tunnel, rather than its hydrophobicity, that confers differential disulfiram reactivity in the two ALDH isozymes. This fits with earlier suggestions that it is their inherent bulkiness and size that predisposes all-*trans* retinal, disulfiram and other compounds to preferential interaction with ALDH1 [45]. A recent study [46] reported that alcoholic patients being treated with disulfiram develop symptoms attributable to a build-up of retinoic acid precursors, suggesting the involvement of ALDH1 in complications associated with disulfiram therapy. With knowledge of both the ALDH1 and ALDH2 structures, it should now be possible to synthesise effective ALDH2 inhibitors that do not interfere with the function of ALDH1.

The change in the conformation of the N-terminal segment and several nearby loops surrounding the entrance to the substrate tunnel suggests that surface differences are important to ALDH structure and function, at least in terms of access to substrate. There is kinetic evidence that retinal-loaded intracellular retinal binding protein (CRBP II) [38] is a good substrate for ALDH1 [5,14]. If, *in vivo*, the retinal substrate is passed directly from CRBP II to ALDH1, it is an attractive idea that the molecular surface of ALDH1 in the vicinity of the substrate tunnel entrance could be important for recognition and binding of CRBP II by ALDH1. Indeed, ALDH1 could also conceivably pass its product, retinoic acid, directly to one of the intracellular retinoic acid binding proteins. However, experimental work is required to show whether there are specific interactions between ALDH1 and retinoid-binding proteins.

Reorientation of NADH as a critical component of the ALDH mechanism

In the ALDH enzymes, NAD^+ binding appears to be both flexible and highly variable for the nicotinamide half of the cofactor. ALDH1, ALDH2 and ALDH3 all exhibit different binding modes for the nicotinamide half of the cofactor, although the adenine moiety interacts with the protein almost identically in all three enzyme structures determined to date. This observation suggests that movement of the nicotinamide ring in and out of the active site is a conserved and important component of the functional enzyme. Our observation that the general base Glu268 also exhibits disorder in ALDH1, and taking into consideration chemical requirements for both the dehydrogenase and deacylation steps of the reaction, leads us to suggest that movement of the NAD^+ cofactor and Glu268 are coupled in the ALDH reaction mechanism. Specifically,

during hydride transfer from the Cys302 thiohemiacetal to the NAD^+ nicotinamide, the sidechain of Glu268 must be 'tucked away' from the nicotinamide ring of the cofactor, as it is primarily observed to be in all ALDH crystal structures. Before deacylation of the thioester can take place, the reduced nicotinamide ring must at least partially exit the active-site pocket to make room for a water molecule to position itself near the thioester carbon atom of the acyl intermediate. Glu268 most likely abstracts a proton from this deacylating water, and would have to move from its modelled position to do this. Hence, we believe that the sidechain of Glu268 has two conformations: a passive conformer that 'stays out of the way' to allow hydride transfer to the nicotinamide, and an active conformer that participates in proton abstraction from a thioester-deacylating water molecule. The active site general base Glu268 [28,33] is buried away from the solvent in the active site, and is too far from Cys302 to act directly as a base [34], hence the necessity for a deacylating water molecule.

An idea that directly follows the requirement for flexibility in NAD^+ binding is that the novel mode of NAD^+ binding in the N-terminal domain of ALDHs somehow facilitates the flexibility required in the nicotinamide half of the cofactor. In contrast to other NAD^+-dependent dehydrogenases, there are few interactions between the NAD^+ phosphates and the protein; especially lacking are lysine or arginine residues at the phosphate-binding site or a strong interaction between the phosphates and the N terminus of a helix dipole. In contrast, there is a patch of strong negative electrostatic potential near the NAD^+ phosphate binding pocket that is conserved, at least between ALDH1 and ALDH2 (Figure 3c). This suggests to us that binding of the pyrophosphate of NAD^+ in ALDH is intentionally weak, so that the phosphates can act as a flexible 'ball-and-socket' swivel, allowing the nicotinamide moiety to adopt different conformations during the individual steps of the reaction pathway.

Biological implications

Retinoic acid is required for the correct formation of many organs and structures during vertebrate development, including the spinal chord, retina and heart. Maintenance of adult epithelial cell type is also mediated by retinoic acid. All of the known effects of retinoic acid are due to the binding of all-*trans* or 9-*cis* retinoic acid to nuclear retinoic acid receptors, which act as transcription factors and regulate gene expression in the cell nucleus. The cytosolic isoform of aldehyde dehydrogenase (ALDH1) is the single most important enzyme for the production of all-*trans* and 9-*cis* retinoic acid in vertebrate cells, and retinal dehydrogenase activity has been shown to localise with high concentrations of retinoic acid during embryonic spinal chord formation. Factors that attenuate retinal dehydrogenase activity in living cells are not well characterised, and it is hoped that structural information pertaining to the retinal-specific ALDH1 isozyme will aid in understanding how the spatiotemporal distributions of retinoic acid are controlled during vertebrate development.

The three-dimensional structure of sheep liver ALDH1 has been determined and compared to that of the mitochondrial ALDH2 isozyme. Comparisons of the two enzymes reveal that the major differences are localised to the substrate-binding tunnel and to the mode of NAD^+ cofactor binding. The size and shape of the ALDH1 substrate entrance tunnel is likely to be the primary determinant of retinal specificity for this enzyme. In contrast, the ALDH2 substrate tunnel is too constricted to accept retinal, and prefers acetaldehyde as a substrate. We contend that the large size of the ALDH1 substrate entrance tunnel relative to ALDH2 is responsible for the increased reactivity *in vitro* of ALDH1 to the alcohol aversive drug disulfiram.

The presence of two discretely ordered conformers of NAD^+ in the ALDH1 structure argues strongly for an enzyme reaction mechanism in which the nicotinamide portion of the cofactor can move in and out of the active-site pocket, tethered to a flexible arm (the nicotinamide phosphate and ribose), while the adenine half of the cofactor acts as a rigid anchor. This observation is in agreement with the two-step nature of the chemistry involved in aldehyde dehydrogenation and enzyme–thioester hydrolysis during the reaction cycle. In this proposed reaction scenario, the general base Glu268 must also be mobile to accommodate productive NAD(H) binding and to function in both thiohemiacetal formation and thioester hydrolysis. The observed disorder of the Glu268 sidechain in all four subunits of the sheep ALDH1 structure supports this hypothesis.

Materials and methods

Isolation, purification and crystallisation of sheep liver ALDH1

Sheep liver cytosolic ALDH was isolated and purified as described previously [47]. Fractions containing active ALDH were identified by enzyme assay using acetaldehyde as substrate and monitoring the appearance of NADH spectrophotometrically at 340 nm. The final fractions were assayed for activity and checked for purity by sodium dodecyl sulphate (SDS) polyacrylamide gel electrophoresis and isoelectric focusing. The purest fractions were then pooled, dialysed against 50 mM Na/K phosphate, pH 7.4, 1 mM DTT and concentrated to 10 mg/ml protein using microconcentrators. Crystals were grown using the hanging-drop vapour diffusion technique as described previously [48]. The protein concentration was 10 mg/ml with 1 mM NAD^+, and the reservoir solution contained 170 mM $MgCl_2$, 100 mM Bis-Tris-propane (pH 6–7) and 6–7% w/v monomethylether polyethylene glycol (PEG) 5000. Drops were typically 4 μl to 6 μl and contained equal volumes of the protein solution and precipitant. The crystals tended to grow over a very narrow PEG concentration and often several trays would only yield one or two usable crystals. We routinely observed three crystal forms: a thin plate habit that belonged to a C-centred orthorhombic lattice (a = 170.8, b = 330.7, c = 80.77 Å) containing one tetramer per asymmetric unit; a cuvette habit that was in space group $P2_12_12$ (a = 92.9, b = 151.3, c = 81.4 Å) with one dimer per asymmetric unit; and a chunky plate habit that was triclinic (a = 80.69, b = 87.62, c = 90.84 Å, α = 110.5, β = 105.6, γ = 103.6°)

and contained a tetramer in the P1 unit cell. Most of the crystals diffracted poorly, either at room temperature or flash frozen at liquid nitrogen temperatures, but about 10% diffracted well. The triclinic crystals were of the best quality, and after flash freezing in mother liquor plus 30% v/v glycerol, diffracted to nearly 2.0 Å resolution. The average mosaic spread for a typical crystal was about 1.0° after freezing. Data for the $P2_12_12$ cell were collected on beamline BL-6A (λ = 1.000 Å) at the Photon Factory, Tsukuba Japan, using imaging plates on a Weissenberg Camera at a temperature of 12°C. Crystals of the triclinic cell were flash frozen at 113K, and diffraction data were recorded using a Rigaku RaxisIIC imaging plate detector, with 0.1 mm collimated Cu-Kα radiation (λ = 1.5418 Å) from a Rigaku RU-200B rotating-anode generator operating at 50 kV, 100 mA. All data were indexed, and integrated with the program DENZO [49] and initially post-refined with SCALEPACK [49] to determine an accurate unit cell. The images were reprocessed with the post-refined cell parameters and individual films were scaled and merged with SCALEPACK. Profile-fitted intensities were converted to amplitudes using the CCP4 program TRUNCATE [50,51].

Structure solution and refinement

The orthorhombic crystal form was first solved by using the refined coordinates of a monomer of bovine ALDH2 (coordinates kindly provided by T Hurley). With data from 10–3.2 Å, the cross-rotation function in AMoRe [52] yielded two clear peaks. The first peak was at Eulerian angles α = 10.71°, β = 60.76°, γ = 88.16° with height 14.8 (rms = 1.7). The second peak was at α = 146.95°, β = 60.35°, γ = 88.17° with a height of 13.3. A translation function in space group $P2_12_12$ (10–3.2 Å data) gave a clear solution for both the first (correlation coefficient = 0.308, R factor = 0.504) and second (correlation coefficient = 0.262, R factor = 0.519) cross-rotation peaks. Fixing the first solution, and searching for the second translation vector resulted in a correlation coefficient of 0.513 and an R factor of 0.431. Rigid-body refinement improved the solutions, yielding a final correlation coefficient of 0.643 (R factor = 0.383). After dissimilar sidechains between sheep ALDH1 and bovine ALDH2 were truncated to alanine, SIGMAA-weighted maps [53] were calculated and many missing sidechains were easily built into the electron-density maps. The maps were of excellent quality, despite the poor merging statistics of the diffraction data (R_{merge} = 0.13). Four rounds of TNT refinement [54,55] using NCS constraints on the two monomers in the crystallographic asymmetric unit, followed by model building into SIGMAA-weighted $2F_o–F_c$ and $F_o–F_c$ maps yielded a free R factor of 31% (for 10% of the data) between 30.0 and 3.1 Å resolution. The working R factor was 26% and one B factor was modelled per residue. At this resolution, it was difficult to fit the NAD^+ electron density unambiguously, but the fitting of the adenine half of the cofactor was relatively straightforward. Once the triclinic data became available, we carried out molecular replacement using the partially refined orthorhombic model. The rotation function solution for the orthorhombic tetramer was straightforward in AMoRe with a peak height of 63 (rms = 2.0); the next highest peak was 10.0. The nature of the rotation solution suggested the triclinic and orthorhombic cells were very closely related. Least squares refinement in TNT using a maximum likelihood target [56] followed by model building and eventual refinement in CNS [57], resulted in a free R factor of 25.8% for a randomly chosen 10% of the data (see Table 1). In all refinements, the bond length and angle parameters of Engh and Huber were used [58]. The quality of the electron-density maps was excellent and a model for the complete polypeptide, excluding residues –1 to 6, was built. Amino acid sidechains for Lys56, Arg86, Lys357, Lys411 and Lys418 were not included in the final model due to apparent disorder, and these amino acids were modelled as alanine. A total of 140 water molecules were added to the tetrameric structure. This corresponded to 35 unique and identical water molecules per ALDH1 monomer. Although high concentrations of Mg^{2+} ions were present in the crystallisation solutions and appeared necessary for growth of ALDH1 crystals, we did not conclusively identify any Mg^{2+} ions in the sheep ALDH1 structure. During positional refinement of the model, strict NCS restraints were maintained giving a final rmsd between monomers of 0.009 Å. Although two conformations of the nicotinamide half of the NAD^+ cofactor were apparent in difference and omit electron-density maps, only the highest occupancy NAD^+ conformer (about 80% occupancy) was used for the structure-factor calculations and least-squares refinement. Analysis of the final coordinates with PROCHECK [59] revealed excellent stereochemistry, with 89% of residues in the most favoured regions and 10.2% in additional allowed regions. The rmsd values for bonds and angles, as well as other refinement statistics, are given in Table 2.

*Modelling of all-*trans *and 9-*cis *retinal in the ALDH1 active site*

All-*trans* retinal and its 9-*cis* isomer were docked into the ALDH1 active site manually, using the retinoic acid coordinates from human CRABP II (PDB code 1CBS) [40]. Solvent-accessible volumes of the tunnels before docking were calculated with the program VOIDOO [60] and solvent-accessible surface areas before and after docking of retinal were calculated using programs in the CCP4 suite [50]. Close contacts were examined and adjusted using TURBO-FRODO [61]. The sidechain of Met120 was manually adjusted to relieve bad contacts for both retinoid complexes. No carbon–carbon contact distances less than 3.4 Å were observed in the modelled retinal complexes. The retinal coordinates were adjusted such that the aldehyde carbonyl carbon made close contact with the Sγ of Cys302 (2.5 Å) in anticipation of thiohemicacetal formation, the aldehyde hydrogen was in a reasonable position for hydride transfer, and the aldehyde carbonyl oxygen was pointing at the presumed oxyanion hole making hydrogen bonds with Cys302 NH and Asn169 Nδ2.

Accession numbers

The atomic coordinates for the triclinic form of sheep liver ALDH1 have been deposited in the Brookhaven Protein Data Bank with accession code 1bxs.

Acknowledgements

This research was supported by the Health Research Council of New Zealand, the Neurological Foundation of New Zealand, the New Zealand Lottery Grants Board in the form of an equipment grant, and by the Howard Hughes Medical Institute through the award of an International Research Scholarship to ENB. We also gratefully acknowledge Thomas Hurley and colleagues for providing the atomic coordinates of bovine ALDH2 prior to their release from the PDB, and Arijit Dasgupta who grew several of the triclinic ALDH1 crystals used in this study.

References

1. Kastner, P., Mark, M. & Chambon, P. (1995). Nonsteroid nuclear receptors: what are genetic studies telling us about their role in real life? *Cell* **83**, 859-869.
2. Mangelsdorf, D.J., *et al.*, & Evans, R.D. (1995). The nuclear receptor superfamily: the second decade. *Cell* **83**, 835-839.
3. Hofmann, C. & Eichele, G. (1994). Retinoids in development. In *The Retinoids: Biology, Chemistry and Medicine, 2nd Ed.* (Sporn, M.B., Roberts, A.B. & Goodman, D.S., eds), pp. 387-441, Raven Press, New York.
4. Duester, G. (1996). Involvement of alcohol dehydrogenase, short-chain dehydrogenase/reductase, aldehyde dehydrogenase, and cytochrome P450 in the control of retinoid signaling by activation of retinoic acid synthesis. *Biochemistry* **35**, 12221-12227.
5. Kitson, K.E. & Blythe, T.J. (1999). The hunt for a retinal-specific aldehyde dehydrogenase. In *Enzymology and Molecular Biology of Carbonyl Metabolism 7.* (Weiner, H., Lindahl, R., Crabb, D.W. & Flynn, T.G., eds), Plenum Press, New York, in press.
6. McCaffery, P. & Drager, U.C. (1994). Hot spots of retinoic acid synthesis in the developing spinal chord. *Proc. Natl Acad. Sci. USA* **91**, 7194-7197.
7. McCaffery, P., Tempst, P., Lara, G. & Drager, U.C. (1991). Aldehyde dehydrogenase is a positional marker in the retina. *Development* **112**, 693-702.
8. Rongnoparut, P. & Weaver, S. (1991). Isolation and characterization of a cytosolic aldehyde dehydrogenase-encoding cDNA from the mouse liver. *Gene* **101**, 261-265.
9. Bhat, P.V., Labrecque, J., Boutin, J.-M., Lacroix, A. & Yoshida, A. (1995). Cloning of a cDNA encoding rat aldehyde dehydrogenase with high activity for retinal oxidation. *Gene* **166**, 303-306.
10. Penzes, P., Wang, X., Sperkova, Z. & Napoli, J.L. (1997). Cloning of a rat cDNA encoding retinal dehydrogenase isozyme type I and its expression in *E. coli*. *Gene* **191**, 167-172.
11. El Akawi, Z. & Napoli, J.L. (1994). Rat liver cytosolic retinal dehydrogenase: comparison of 13-*cis*, 9-*cis*, and all-*trans*-retinal as substrates and effects of cellular retinoid-binding proteins and retinoic acid on activity. *Biochemistry* **33**, 1938-1943.

12. Labrecque, F., Dumas, F., Lacroix, A. & Bhat, P.V. (1995). A novel isoenzyme of aldehyde dehydrogenase specifically involved in the biosynthesis of 9-*cis* and all-*trans* retinoic acid. *Biochem. J.* **305**, 681-684.
13. Zhao, D., *et al*., & Drager, U.C. (1996). Molecular identification of a major retinoic-acid-synthesizing enzyme, a retinaldehyde-specific dehydrogenase. *Eur. J. Biochem.* **240**, 15-22.
14. Wang, X., Penzes, P. & Napoli, J.L. (1996). Cloning of a cDNA encoding an aldehyde dehydrogenase and its expression in *Escherichia coli. J. Biol. Chem.* **271**, 16288-16293.
15. Yoshida, A., Hsu, L.C. & Yasunami, M. (1991). Genetics of human alcohol-metabolizing enzymes. *Prog. Nucleic Acids Res. Mol. Biol.* **40**, 255-285.
16. Yoshida, A., Hsu, L.C. & Dave, V. (1992). Retinal oxidation activity and biological role of human cytosolic aldehyde dehydrogenase. *Enzyme* **46**, 239-244.
17. Klyosov, A.A. (1996). Kinetics and specificity of human liver aldehyde dehydrogenases toward aliphatic, aromatic, and fused polycyclic aldehydes. *Biochemistry* **35**, 4457-4467.
18. Klyosov, A.A., Rashkovetsky, L.G., Tahir, M.K. & Keung, W.-M. (1996). Possible role of liver cytosolic and mitochondrial aldehyde dehydrogenases in acetaldehyde metabolism. *Biochemistry* **35**, 4445-4456.
19. Yoshida, A., Huang, I.-Y. & Ikawa, M. (1984). Molecular abnormality of an inactive aldehyde dehydrogenase variant commonly found in orientals. *Proc. Natl Acad. Sci. USA* **81**, 258-261.
20. Crabb, D.W., Edenberg, H.J., Bosron, W.F. & Li, T.-K. (1989). Genotypes for aldehyde dehydrogenase deficiency and alcohol sensitivity. The inactive ALDH2 allele is dominant. *J. Clin. Invest.* **83**, 314-316.
21. Farres, J., Wang, X., Takahashi, K., Cunningham, S.J., Wang, T.T. & Weiner, H. (1994). Effects of changing glutamate 487 to lysine in rat and human liver mitochondrial aldehyde dehydrogenase. *J. Biol. Chem.* **269**, 13854-13860.
22. Wang, X., Sheikh, S., Saigal, D., Robinson, L. & Weiner, H. (1997). Heterotetramers of human liver mitochondrial (Class 2) aldehyde dehydrogenase expressed in *Escherichia coli. J. Biol. Chem.* **271**, 31172-31178.
23. Liu, Z.-J., *et al*., & Wang, B.-C. (1997). The first structure of an aldehyde dehydrogenase reveals novel interactions between NAD and the Rossmann fold. *Nat. Struct. Biol.* **4**, 317-326.
24. MacGibbon, A.K.H., Blackwell, L.F. & Buckley, P.D. (1977). Kinetics of sheep-liver cytoplasmic aldehyde dehydrogenase. *Eur. J. Biochem.* **77**, 93-100.
25. MacGibbon, A.K.H., Buckley, P.D. & Blackwell, L.D. (1977). Evidence for two-step binding of reduced nicotinamide adenine dinucleotide to aldehyde dehydrogenase. *Biochem. J.* **165**, 455-462.
26. Hart, G.J. & Dickinson, F.M. (1982). Kinetic properties of highly purified preparations of sheep liver cytoplasmic aldehyde dehydrogenase. *Biochem. J.* **203**, 617-627.
27. Blackwell, L.F., Motion, R.L., MacGibbon, A.K.H., Hardman, M.J. & Buckley, P.D. (1987). Evidence that the slow conformation change controlling NADH release for the enzyme is rate-limiting during the oxidation of propionaldehyde by aldehyde dehydrogenase. *Biochem. J.* **242**, 803-808.
28. Abriola, D.P., Fields, R., Stein, S., MacKerell, A.D. & Pietruszko, R. (1987). Active site of human liver aldehyde dehydrogenase. *Biochemistry* **26**, 5679-5684.
29. Kitson, T.M., Hill, J.P. & Midwinter, G.G. (1991). Identification of a catalytically essential nucleophilic residue in sheep liver cytoplasmic aldehyde dehydrogenase. *Biochem. J.* **275**, 207-210.
30. Farres, J., Wang, T.T.Y., Cunningham, S.J. & Weiner, H. (1995). Investigation of the active site cysteine residue of rat liver mitochondrial aldehyde dehydrogenase by site-directed mutagenesis. *Biochemistry* **34**, 2592-2598.
31. Jones, K.M., Kitson, T.M., Kitson, K.E., Hardman, M.J. & Tweedie, J.W. (1995). Human Class 1 aldehyde dehydrogenase, expression and site directed mutagenesis. In *Enzymology and Molecular Biology of Carbonyl Metabolism.* (Weiner, H., Holmes, R.S. & Wermuth, B., eds), Vol. 5, pp. 17-23. Plenum Press, New York.
32. Harper Jones, K., Lindahl, R., Baker, D.C. & Timkovich, R. (1987). Hydride transfer stereospecificity of rat liver aldehyde dehydrogenase. *J. Biol. Chem.* **262**, 10911-10913.
33. Wang, X. & Weiner, H. (1995). Involvement of glutamate 268 in the active site of human liver mitochondrial (Class 2) aldehyde dehydrogenase as probed by site-directed mutagenesis. *Biochemistry* **34**, 237-243.
34. Steinmetz, C.G., Xie, P., Weiner, H. & Hurley, T.D. (1997). Structure of mitochondrial aldehyde dehydrogenase: the genetic component of ethanol aversion. *Structure* **5**, 701-711.
35. Bourguet, W., Ruff, M., Chambon, P., Gronemeyer, H. & Moras, D. (1995). Crystal structure of the ligand-binding domain of the human nuclear receptor RXR-α. *Nature* **375**, 377-382.
36. Renaud, J.-P., *et al*., & Moras, D. (1995). Crystal structure of the RAR-γ ligand-binding domain bound to all-*trans* retinoic acid. *Nature* **378**, 681-689.
37. Cowan, S.W., Newcomer, M.E. & Jones, T.A. (1993). Crystallographic studies on a family of cellular lipophilic transport proteins. *J. Mol. Biol.* **230**, 1225-1246.
38. Winter, N.S., Bratt, J.M. & Banaszak, L.J. (1993). Crystal structures of holo and apo-cellular retinol-binding protein II. *J. Mol. Biol.* **230**, 1247-1259.
39. Newcomer, M.E. (1993). Structure of the epididymal retinoic acid binding protein at 2.1 Å resolution. *Structure* **1**, 7-18.
40. Kleywegt, G.J., *et al*., & Jones, T.A. (1994). Crystal structures of cellular retinoic acid binding proteins I and II in complex with all-*trans*-retinoic acid and a synthetic retinoid. *Structure* **2**, 1241-1258.
41. Staynor, C.K & Tweedie, J.W. (1995). Cloning and characterization of the cDNA for sheep liver cytosolic aldehyde dehydrogenase. In *Enzymology and Molecular Biology of Carbonyl Metabolism.* (Weiner, H., Holmes, R.S. & Wermuth, B., eds), Vol. 5, pp. 61-66, Plenum Press, New York.
42. Vallari, R.C. & Pietruszko, R. (1982). Human aldehyde dehydrogenase: mechanism of inhibition by disulfiram. *Science* **216**, 637-639.
43. Kitson, T.M. (1983). Mechanism of inactivation of sheep liver cytoplasmic aldehyde dehydrogenase by disulfiram. *Biochem. J.* **213**, 551-554.
44. Lam, J.P., Mays, D.C. & Lipsky, J.J. (1997). Inhibition of recombinant human mitochondrial and cytosolic aldehyde dehydrogenases by two candidates for the active metabolites of disulfiram. *Biochemistry* **36**, 13748-13754.
45. Kitson, T.M. & Kitson, K.E. (1997). The action of cytosolic aldehyde dehydrogenase on resorufin acetate. In *Enzymology and Molecular Biology of Carbonyl Metabolism*. (Lindahl, R., Crabb, D.W. & Flynn, T.G., eds), Vol. 6, pp. 201-208, Plenum Press, New York.
46. Santonastaso, M., Cecchetti, E., Pace, M. & Piccolo, D. (1997). Yellow palms with disulfiram. *Lancet* **350**, 266.
47. Kitson, T.M. & Kitson, K.E. (1994). Probing the active site of cytoplasmic aldehyde dehydrogenase with a chromophoric reporter group. *Biochem. J.* **300**, 25-30.
48. Baker, H.M., *et al*., & Baker, E.N. (1994). Crystallization and preliminary X-ray diffraction studies on cytosolic (Class 1) aldehyde dehydrogenase from sheep liver. *J. Mol. Biol.* **241**, 263-264.
49. Otwinowski, Z. & Minor, W. (1997). Processing of X-ray diffraction data collected in oscillation mode. *Methods Enzymol.* **276**, 307-326.
50. *Collaborative Computational Project Number 4*. (1994). The CCP4 suite: programs for protein crystallography. *Acta Cryst. D* **50**, 760-763.
51. French, S. & Wilson, K. (1978). On the treatment of negative intensity observations. *Acta Cryst. A* **34**, 517-525.
52. Navaza, J. & Saludjian, P. (1997). AMoRe: an automated molecular replacement program package. *Methods Enzymol.* **276**, 581-594.
53. Read, R.J. (1986). Improved Fourier coefficients for maps using phases from partial structures with errors. *Acta Cryst. A* **42**, 140-149.
54. Tronrud, D.E., Ten Eyck, L.F. & Matthews, B.W. (1987). An efficient general-purpose least squares refinement program for macromolecular structures. *Acta Cryst. D* **52**, 743-748.
55. Tronrud, D.E. (1992). Conjugate-direction minimization: an improved method for refinement of macromolecules. *Acta Cryst. A* **48**, 912-916.
56. Pannu, N.S. & Read, R.J. (1996). Improved structure refinement through maximum likelihood. *Acta. Cryst. A* **52**, 659-668.
57. Adams, P.D., Pannu, N.S., Read, R.J. & Brünger, A.T. (1997). Cross-validated maximum likelihood enhances crystallographic simulated annealing refinement. *Proc. Natl Acad. Sci. USA* **94**, 5018-5023.
58. Engh, R.A. & Huber, R. (1991). Accurate bond and angle parameters for X-ray protein structure refinement. *Acta Cryst. A* **47**, 392-400.
59. Laskowski, R.A., MacArthur, M.W., Moss, D.S. & Thornton, J.M. (1993). PROCHECK: a program to check the stereochemical quality of protein structures. *J. Appl. Cryst.* **26**, 283-291.
60. Kleywegt, G.J. & Jones, T.A. (1994). Detection, delineation, measurement and display of cavities in macromolecular structures. *Acta Cryst. D* **50**, 178-185.
61. Roussel, A. & Cambillau, C. (1991). TURBO-FRODO, Silicon Graphics applications directory. Silicon Graphics, Mountain View, California.
62. Nicholls, A., Sharp, K.A. & Honig, B. (1991). Protein folding and association: insights from the interfacial and thermodynamic properties of hydrocarbons. *Proteins* **11**, 281-296.